Multiscale Imaging of Nuclear Deformation at the Electron-Ion Collider

Heikki Mäntysaari,[1,2] Björn Schenke,[3] Chun Shen,[4,5] and Wenbin Zhao[4]
[1]*Department of Physics, University of Jyväskylä, P.O. Box 35, 40014 University of Jyväskylä, Finland*
[2]*Helsinki Institute of Physics, P.O. Box 64, 00014 University of Helsinki, Finland*
[3]*Physics Department, Brookhaven National Laboratory, Upton, New York 11973, USA*
[4]*Department of Physics and Astronomy, Wayne State University, Detroit, Michigan 48201, USA*
[5]*RIKEN BNL Research Center, Brookhaven National Laboratory, Upton, New York 11973, USA*

(Received 15 March 2023; revised 14 June 2023; accepted 17 July 2023; published 7 August 2023)

We show within the color glass condensate framework that exclusive vector meson production at high energy is very sensitive to the geometric deformation of the target nucleus at multiple length scales. We show that different multipole deformation parameters affect different regions of transverse momentum transfer. These results have two important consequences: (1) Deformations of nuclear targets need to be taken into account when making predictions for and interpreting certain observables at the EIC. (2) Differential diffractive vector meson production has the potential to become a powerful tool, enabling the most direct measurements of nuclear structure at different length scales, ranging from large scale nuclear deformation at low transverse momentum transfer to fluctuations on nucleon- and subnucleon-size scales at higher transverse momentum transfer.

DOI: 10.1103/PhysRevLett.131.062301

Introduction.—Understanding the geometric structures of the proton and nuclei, including their event-by-event fluctuations, is of fundamental interest. Deep inelastic scattering (DIS) of leptons on hadrons is one of the most important tools to probe the partonic structure of protons and nuclei. In the 2030s, the Electron-Ion Collider (EIC) in the U.S. will provide access to nuclear-DIS for the first time in collider kinematics [1,2]. In addition to the EIC, there are also other longer-term proposals for future nuclear-DIS facilities at CERN [3] and in China [4].

Exclusive vector meson (e.g., J/ψ) production off nucleons and nuclei is a particularly clean and powerful process to probe the nuclear high-energy structure at small longitudinal momentum fraction x for several reasons. First, in order to produce only the vector meson and nothing else, net color charge cannot be transferred to the target, and the final state is unambiguously identified by a large rapidity gap, i.e., a wide range in rapidity where no particles are produced. This also requires that at least two gluons are exchanged, which renders the cross section approximately proportional to the squared gluon distribution [5] at leading order (see Ref. [6] for a recent analysis at next-to-leading order accuracy). Additionally, only in such exclusive scattering is it possible to determine the total momentum transfer to the target hadron or nucleus, which is the Fourier conjugate to the impact parameter and as such provides access to the target geometry.

In the hot QCD community, understanding the spatial shape of colliding objects in heavy-ion collisions is a necessary input when the deconfined quark-gluon plasma (QGP) state is probed [7]. The initial nucleon and nuclear geometry determine the spatial distribution of nuclear matter in the collision, which in turn determines the initial pressure anisotropies that are transformed into observable momentum space correlations when the space-time evolution of the QGP is simulated. The hydrodynamic modeling of heavy-ion collisions with an accurate initial state description in collisions of several different ion species has revealed how the detailed structural properties of the colliding nuclei are visible in final state particle correlations [8–19].

The study of collisions involving heavy ions at the Relativistic Heavy Ion Collider (RHIC), the Large Hadron Collider (LHC), and the future EIC offers a synergistic approach to understanding the properties of high-energy nuclei and hot and dense nuclear matter. The EIC will probe in detail the small-x structure of the nuclei (x being the longitudinal momentum fraction of the partons inside; higher energy processes probe smaller x), obtaining fundamentally interesting information and constraining the initial state of heavy-ion collisions [20–22]. In turn, as mentioned above, heavy-ion collisions can themselves constrain the high-energy structure of nuclei, including deformation and nucleon clustering. The complementary information from these facilities is essential for gaining a complete picture of the properties of the QGP, and the influence of nuclear geometry in the initial state.

We employ the color glass condensate framework [23] supplemented with a model that describes the nuclear geometry including nucleon substructure in terms of gluonic hot spots [22]. Recently, in Ref. [24], we performed a statistically rigorous Bayesian analysis to extract the

© 2023 American Physical Society

posterior likelihood distribution for the model parameters describing the event-by-event fluctuating proton geometry from HERA J/ψ production data [25]. In this Letter, we extend our studies to $e+A$ collisions and for the first time explore the effects of nuclear deformation on the diffractive cross sections for large nuclei. Specifically, we study the dependence of the $|t|$ differential diffractive J/ψ cross sections on the deformation parameters of uranium. To examine how energy evolution modifies the effects of deformation, we perform numerical simulations solving the Jalilian-Marian, Iancu, McLerran, Weigert, Leonidov and Kovner (JIMWLK) equations (see, e.g., Ref. [26]) to evolve the nuclear configurations to smaller x.

We further study vector meson production in electron scattering off smaller nuclei. Of particular interest are ^{20}Ne and ^{16}O, which have a similar mass number, but are expected to differ in shape. Calculations in different models [27–31] obtain a characteristic bowling pin shape for ^{20}Ne, essentially forming a ^{16}O like structure with an additional α cluster in its periphery. We provide model predictions for future EIC measurements, in particular for the ratio of the $|t|$ differential diffractive J/ψ production cross sections in the two systems.

Vector meson production at high energy.—The total diffractive cross section in DIS gives insight into the total small-x gluon densities of the target nuclei. More differential observables such as the exclusive production of a vector meson, $\gamma^*+p/A\to V+p/A$, as a function of (squared) momentum transfer $-t$ can provide more detailed information on the target structure. The coherent cross section, corresponding to the process where the target remains in the same quantum state, can be obtained by averaging over the target color charge configurations Ω at the amplitude level [32]:

$$\frac{\mathrm{d}\sigma^{\gamma^*+A\to V+A}}{\mathrm{d}|t|}=\frac{1}{16\pi}|\langle\mathcal{A}\rangle_\Omega|^2. \tag{1}$$

The incoherent vector meson production cross section, for which the final state of the target is different from its initial state, is obtained by subtracting the coherent contribution from the total diffractive vector meson production cross section [22,33,34]. The incoherent cross section thus has the form of a variance:

$$\frac{\mathrm{d}\sigma^{\gamma^*+A\to V+A^*}}{\mathrm{d}|t|}=\frac{1}{16\pi}[\langle|\mathcal{A}|^2\rangle_\Omega-|\langle\mathcal{A}\rangle_\Omega|^2]. \tag{2}$$

Here $\mathcal{A}$ is the scattering amplitude for diffractive vector meson production, which at high energy describes the splitting of the virtual photon into a quark antiquark pair, the pair's subsequent interaction with the target, followed by the formation of the vector meson. It can be written as [35,36] (see also Refs. [37,38] for recent developments toward next to leading order (NLO) accuracy)

$$\mathcal{A}=2i\int \mathrm{d}^2\mathbf{r}_\perp \mathrm{d}^2\mathbf{b}_\perp \frac{\mathrm{d}z}{4\pi}e^{-i[\mathbf{b}_\perp-(\frac{1}{2}-z)\mathbf{r}_\perp]\cdot\mathbf{\Delta}_\perp} \times[\Psi_V^*\Psi_\gamma](Q^2,\mathbf{r}_\perp,z)N_\Omega(\mathbf{r}_\perp,\mathbf{b}_\perp,x_\mathbb{P}). \tag{3}$$

Here $\mathbf{r}_\perp$ is the transverse size of the $q\bar{q}$ dipole, $\mathbf{b}_\perp$ is the impact parameter measured relative to the target center, and Q^2 is the photon virtuality. The fraction of the large photon plus momentum carried by the quark is given by z, $x_\mathbb{P}$ (which in diffractive processes corresponds to the previously discussed x variable) is the fraction of the target longitudinal momentum transferred to the meson in the frame where the target has a large momentum, and $\mathbf{\Delta}_\perp$ is the transverse momentum transfer, with $-t\approx\mathbf{\Delta}_\perp^2$. The $\gamma^*\to q\bar{q}$ splitting is described by the virtual photon light front wave function Ψ_γ [39]. The vector meson wave function Ψ_V is nonperturbative and needs to be modeled, introducing some uncertainty. Here, we use the Boosted Gaussian parametrization from [35], where the model parameters are constrained by the decay width data.

Dependence on the small-x structure of the target is included in the dipole amplitude $N_\Omega(\mathbf{r}_\perp,\mathbf{b}_\perp,x_\mathbb{P})$, which, for a given target color charge configuration Ω, is $N_\Omega(\mathbf{r}_\perp,\mathbf{b}_\perp,x_\mathbb{P})=1-(1/N_c)\mathrm{tr}\{V[\mathbf{b}_\perp+(\mathbf{r}_\perp/2)]V^\dagger[\mathbf{b}_\perp-(\mathbf{r}_\perp/2)]\}$. The $V(\mathbf{x}_\perp)$ represents a Wilson line, depending on Ω and $x_\mathbb{P}$, and describing the color rotation of a quark state when propagating through the target field at transverse coordinate $\mathbf{x}_\perp$. The Wilson lines are obtained in the same way as in the IP-Glasma initial state description [40] used, e.g., in Refs. [20,21,41–45]. They are computed by first relating the average square color charge density to the local saturation scale extracted from the impact parameter dependent dipole saturation model (IPSat) dipole-proton amplitude [46]. Then, by solving the Yang-Mills equations for the gluon fields, one obtains

$$V(\mathbf{x}_\perp)=\mathrm{P}_-\left\{\exp\left(-ig\int_{-\infty}^{\infty}\mathrm{d}z^-\frac{\rho^a(x^-,\mathbf{x}_\perp)t^a}{\mathbf{\nabla}^2-m^2}\right)\right\}, \tag{4}$$

where P_- represents path ordering in the x^- direction and ρ^a is the color charge density. Here, we introduced the infrared regulator m, which is needed to avoid the emergence of unphysical Coulomb tails.

We note that in the incoherent cross section [Eq. (2)], the square of the impact parameter dependent scattering amplitude is equivalent to the Fourier transform of the two-point function of the nuclear thickness function, which clarifies the sensitivity of this quantity to the target structure at different length scales, depending on $|t|$ (see also Refs. [34,47]).

In this Letter we use subnucleonic fluctuations of the nucleon, introducing an event-by-event fluctuating density by following Refs. [20,21] and writing the density profile of nucleons $T_p(\mathbf{b}_\perp)$ as

$$T_p(\mathbf{b}_\perp) = \frac{1}{N_q}\sum_{i=1}^{N_q} p_i T_q(\mathbf{b}_\perp - \mathbf{b}_{\perp,i}), \tag{5}$$

where the single hot spot density distribution $T_q(\mathbf{b}_\perp) = (1/2\pi B_q)e^{-\mathbf{b}_\perp^2/(2B_q)}$ and the coefficient p_i allows for different normalizations for individual hot spots. It follows the log-normal distribution with the width σ controlling the magnitude of the density fluctuations. Our prescription corresponds to having N_q hot spots with hot spot width B_q. The hot spot positions $\mathbf{b}_{\perp,i}$ are sampled from a two-dimensional Gaussian distribution whose width is denoted by B_{qc}, and the center of mass is shifted to the origin at the end. In this Letter, we use the maximum *a posteriori* parameter set from Bayesian analysis where the geometry parameters at $x_{\mathbb{P}} \approx 0.0017$ are constrained by the exclusive J/ψ production data from HERA [24].

To model the geometric shape of large nuclei, we first sample nucleon positions from a Woods-Saxon distribution

$$\rho(r,\theta) = \frac{\rho_0}{1+\exp[(r-R'(\theta))/a]}, \tag{6}$$

with $R'(\theta) = R[1+\beta_2 Y_2^0(\theta) + \beta_3 Y_3^0(\theta) + \beta_4 Y_4^0(\theta)]$, and ρ_0 is the nuclear density at the center of the nucleus. Here R is the radius parameter and a the skin diffuseness, and θ is the polar angle. A random rotation is applied after the sampling process. The spherical harmonic functions $Y_l^m(\theta)$ and the parameters β_i account for the possible deformation from a spherical shape. The default Woods-Saxon parameters for uranium are $\beta_2 = 0.28$, $\beta_3 = 0$, $\beta_4 = 0.093$, $a = 0.55$ fm, and $R = 6.81$ fm [8–13]. Following Refs. [13,48], we further impose a minimal distance of $d_{\min} = 0.9$ fm between nucleons when sampling in three dimensions. When a nucleon is added and violates the minimum distance criterion with one or more already sampled nucleons, we resample its azimuthal angle ϕ to keep the distributions of radial distances and polar angles unchanged [48]. We note that the choice of model used to describe nuclear deformation is not important for the general points we make in this Letter.

We also study smaller nuclei below. For the case of the nucleon density distribution of ^{20}Ne, we use results from the *ab initio* projected generator coordinate method (PGCM) [30,31,49,50]. In the PGCM one considers a many-body wave function that is a linear superposition of the intrinsic states across the plane of deformation parameters, projected onto quantum numbers reflecting the symmetries of the nuclear Hamiltonian [51–53].

We also compare to the case of a spherical ^{20}Ne nucleus described by a Woods-Saxon distribution with parameters obtained in low-energy electron-nucleus scattering [54]. In this case the parameters are the radius $R = 2.8$ fm, and skin depth $a = 0.57$ fm. For ^{16}O we employ the nucleon density distribution used in Ref. [55], which is obtained from a variational Monte Carlo method using the Argonne v18 two-nucleon potential + UIX interactions [56].

Sensitivity of exclusive scattering to nuclear deformations.—Equation (1) shows that the coherent cross section is sensitive to the average scattering amplitude and as such probes the average structure of the target. The incoherent cross section, Eq. (2), measures the scattering amplitude fluctuations between the different possible color charge configurations. Measuring the total momentum transfer $\mathbf{\Delta}_\perp$ allows one to constrain the geometry fluctuations in the

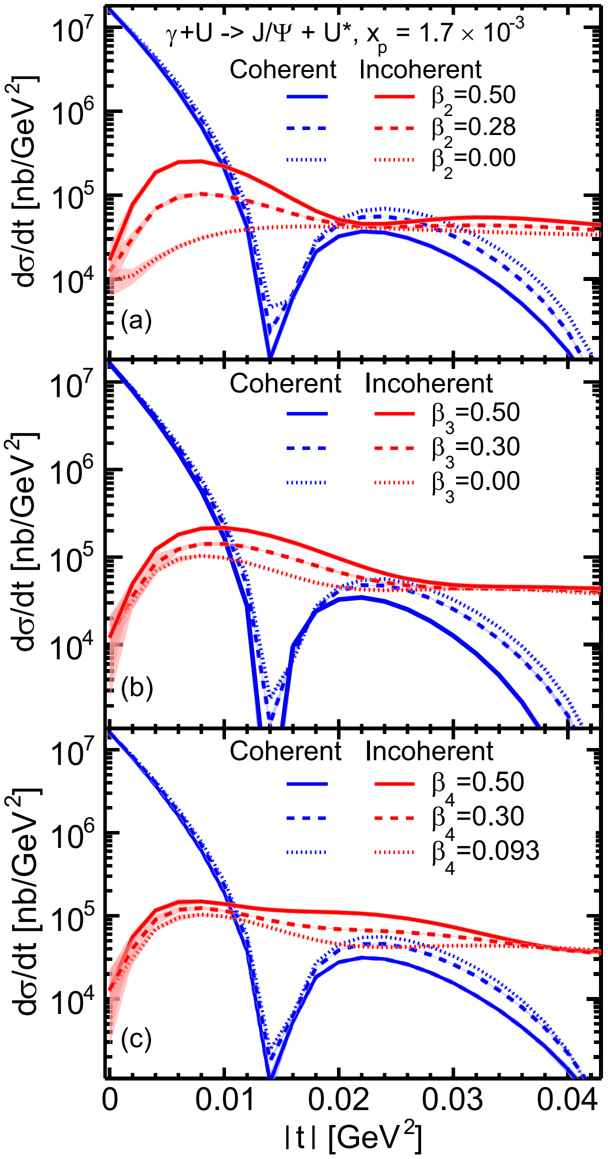

FIG. 1. Coherent and incoherent J/ψ photoproduction cross sections at $x_p = 1.7\times10^{-3}$ in e + U collisions for different β_2 (a), β_3 (b), and β_4 (c) values. The bands show the statistical uncertainty of the calculation.

target at length scales $\sim 1/\sqrt{-t}$. To determine how sensitive the future EIC measurements are to the nuclear deformations in the currently unexplored small-x region, we vary one of the Woods-Saxon deformation parameters β_2, β_3, or β_4 of uranium, while keeping the others set to their default values.

Figure 1 shows the effect of different levels of quadrupole (β_2), octupole (β_3), and hexadecapole (β_4) deformation on the coherent and incoherent $\gamma^* + U \rightarrow \mathrm{J}/\psi + U^{(*)}$ cross sections for a photon virtuality of $Q^2 = 0\ \mathrm{GeV}^2$. Increasing the degree of deformation leads to increasing incoherent cross sections. For example, with a realistic $\beta_2 = 0.28$ the incoherent cross section at $|t| \sim 0.01\ \mathrm{GeV}^2$ is increased by a factor of ~ 5 compared with the case with an assumed spherical uranium target with $\beta_2 = 0.0$. This large enhancement is a result of the random orientations of the deformed nucleus in the laboratory frame leading to larger density fluctuations of the configurations projected onto the transverse plane, which causes larger event-by-event fluctuations in the scattering amplitude.

Importantly, the different types of deformations manifest in different $|t|$ regions and can as such be probed separately at the EIC. The β_2 modifies the incoherent cross section in the smallest $|t| \lesssim 0.015\ \mathrm{GeV}^2$ region. On the other hand, β_3 is important in the range $0.005\ \mathrm{GeV}^2 \lesssim |t| \lesssim 0.025\ \mathrm{GeV}^2$, and β_4 for $0.015\ \mathrm{GeV}^2 \lesssim |t| \lesssim 0.035\ \mathrm{GeV}^2$. These effects take place in different $|t|$ ranges because, for example, the quadrupole deformation β_2 controls the geometric deformation of the target at the longest length scale among these three deformation parameters, which translates into the smallest $|t|$ region in momentum space.

The slope of the coherent cross section at low $|t|$ and the position of the first diffractive minimum are not significantly modified by the deformations, which means that the average size of the uranium nucleus is not modified. However, the deformations do affect the coherent spectrum, especially at higher $|t|$. This is due to the fact that (the projection of) the average density profile is different from that of the spherical nucleus when we have nonzero deformation parameters β_i. Consequently, in addition to the incoherent cross section, the coherent cross section in the relatively large $|t|$ region (after the first diffractive minimum) can be used to access deformations at the EIC.

In order to justify the use of deformation parameters extracted in low-energy experiments to the situation of high-energy scattering, and in particular to see whether the nuclear deformations are washed out at small x, we apply the perturbative JIMWLK evolution equation [26] as in Refs. [41,45] to describe the Bjorken-x dependence of the uranium structure. The uranium configurations at the initial $x_{\mathbb{P}} = 1.7 \times 10^{-3}$ are generated using the same three different β_2 values as above, and default values are used for β_3 and β_4. Figure 2 shows the incoherent-to-coherent cross section ratio as a function of $x_{\mathbb{P}}$, with the total (in)coherent cross sections integrated within $0.0 < |t| < 0.5\ \mathrm{GeV}^2$. This ratio effectively suppresses the uncertainties originating from the modeling of the J/ψ wave function [57]. The decreasing ratio toward small $x_{\mathbb{P}}$ implies that the incoherent cross section grows more slowly than the coherent one with increasing energy, because the event-by-event fluctuations are reduced by the evolution [45] (see also Refs. [41,58]). The difference in the cross section ratio between the different initial quadrupole deformations remains similar throughout the evolution. We conclude that the fluctuations in the nuclear geometry originating from the deformed structure are not washed out by the JIMWLK evolution, and as such we expect the deformations previously inferred from low-energy experiments to also be visible in high-energy electron-ion collisions at the EIC.

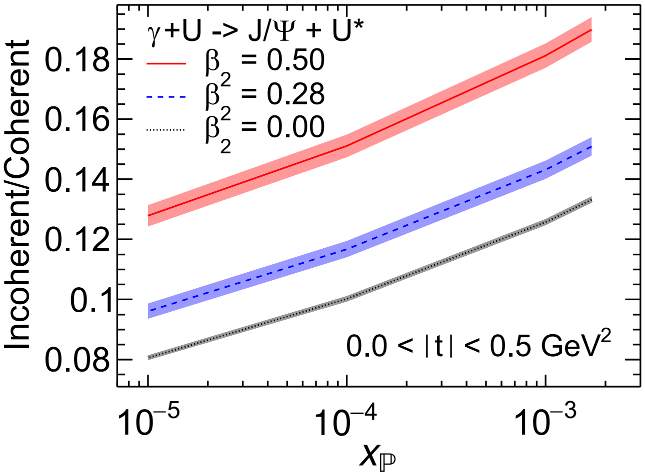

FIG. 2. Incoherent-to-coherent J/ψ photoproduction cross section ratio as a function of $x_{\mathbb{P}}$ in $\mathrm{e}+U$ collisions at different initial β_2 values.

Let us next demonstrate the possibility to probe deformations in the high-energy structure of light nuclei at the EIC, focusing on $^{20}\mathrm{Ne}$ and $^{16}\mathrm{O}$ (see also Ref. [43] where deuteron and helium were considered). Figure 3 shows both the coherent and incoherent J/ψ photoproduction cross sections at $x_{\mathbb{P}} = 1.7 \times 10^{-3}$ off a $^{20}\mathrm{Ne}$ nucleus computed from the *ab initio* PGCM method [30,49,50], which resembles the shape of a bowling pin. They are compared to the case where we neglect all deformations and use a Woods-Saxon distribution as well as to the case of a $^{16}\mathrm{O}$ target, described as discussed above.

Consistent with the uranium case shown in Fig. 1, the bowling-pin-like shape deformations enhance the incoherent cross section when the PGCM $^{20}\mathrm{Ne}$ is compared to the spherical one at small $|t| \lesssim 0.05\ \mathrm{GeV}^2$. To make the enhancement more visible (and to remove some model uncertainties, e.g., from the J/ψ wave function), the bottom panel of Fig. 3 shows the ratio of the incoherent cross sections for both $^{20}\mathrm{Ne}$ cases to the $^{16}\mathrm{O}$ case. We find that in the case of the PGCM $^{20}\mathrm{Ne}$ target, there is an enhancement of up to a factor of 2.7, compared with 1.5 when comparing

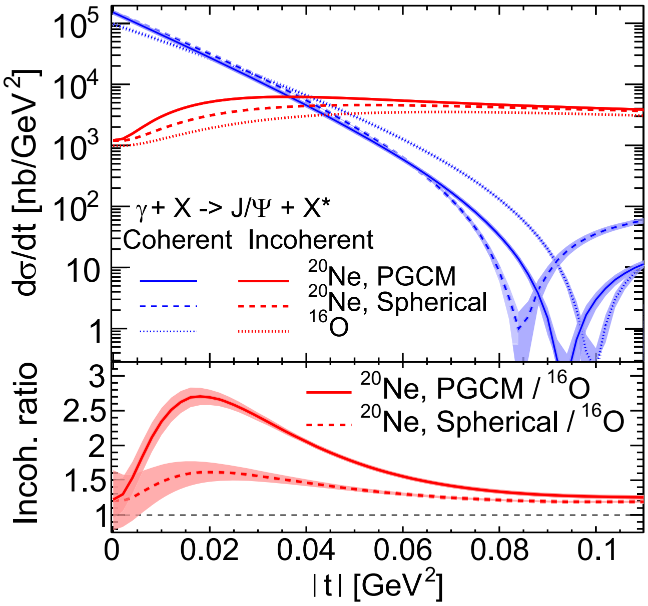

FIG. 3. Coherent and incoherent J/ψ photoproduction cross sections in $e + {}^{20}$Ne and $e + {}^{16}$O collisions (top panel), and the incoherent cross section ratios between ^{20}Ne and ^{16}O (bottom panel).

spherical neon to oxygen. The reason for the enhancement of spherical neon compared to oxygen may simply be the larger size of ^{20}Ne, which is also visible in the locations of the first diffractive minima in the coherent spectra. The additional enhancement for the case of the PGCM ^{20}Ne nucleus is a result of its bowling pin shape, which essentially results from adding a fifth alpha cluster to the four clusters in ^{16}O.

The largest enhancement is in the regime where the coherent cross section dominates; however, even for $|t| \approx 0.05$ GeV^2 where the incoherent cross section begins to dominate the incoherent cross section of ^{20}Ne is almost a factor of 2 larger than that of ^{16}O. At high $|t|$, the incoherent cross sections only differ by a factor of 20/16 originating from the different nuclear mass numbers that affect the overall normalization. This means that the short distance scale fluctuations are identical in oxygen and neon, as it was assumed when constructing the model.

If such measurements can be performed with enough precision at the EIC, they will provide the most direct access to date to the structure of nuclei over all relevant length scales, from nucleus to subnucleon size scales.

Summary.—We have demonstrated that the coherent and incoherent exclusive vector meson production measurements in $e + A$ collisions are affected by the deformed structure of light and heavy ions. In particular, we have shown that quadrupole, octupole, and hexadecapole deformations can significantly modify the incoherent J/ψ production cross section. Different deformations, on different length scales, affect different regions of momentum transfer, and as such can be explored separately at the EIC. We also used numerical solutions to the JIMWLK equation to describe the evolution of the uranium fluctuating structure with decreasing $x_{\mathbb{P}}$, and found that the evolution suppresses the incoherent cross section at high energies, but does not significantly reduce the effects of the initial deformations.

The comparison between the ^{20}Ne nucleus obtained in modern PGCM calculations and the spherical ^{20}Ne or ^{16}O shows that for light ions a nontrivial shape also results in enhanced incoherent cross sections at low $|t|$. The strongest effect was observed in a $|t|$ region where the coherent cross section dominates, but even in the range where the incoherent cross section is dominant, a factor of 2 enhancement was observed between PGCM ^{20}Ne and ^{16}O. We conclude that correctly predicting cross sections for diffractive vector meson production and interpreting future data from the EIC require careful consideration of the nuclear deformation of the studied target. We found modifications of cross sections of up to 200% by including realistic deformations compared with results for an assumed spherical nucleus. Even more importantly, the predicted large sensitivity of the incoherent cross section to deformations at low $|t|$, along with the previously observed sensitivity to the structure at nucleon and subnucleon size scales at higher $|t|$, implies that this observable carries an unprecedented wealth of information on nuclear structure over the entire range of relevant size scales.

This information will be complementary to that obtained from low-energy nuclear structure experiments. It will further have direct applications in heavy-ion collisions at RHIC, LHC, and other future facilities.

We acknowledge Benjamin Bally, Thomas Duguet, Jean-Paul Ebran, Mikael Frosini, Giuliano Giacalone, Govert Nijs, Tomás Rodriguez, Vittorio Somà, and Wilke van der Schee for kindly sharing unpublished results on the ground-state density of ^{20}Ne. We also thank Giuliano Giacalone for useful discussions, and acknowledge two EMMI Rapid Reaction Task Force meetings on “Nuclear physics confronts relativistic collisions of isobars” at Heidelberg University. We thank the Institute for Nuclear Theory at the University of Washington for its kind hospitality and stimulating research environment. This research was supported in part by the INT’s U.S. Department of Energy Grant No. DE-FG02-00ER41132. B. P. S. and C. S. are supported by the U.S. Department of Energy, Office of Science, Office of Nuclear Physics, under DOE Contract No. DE-SC0012704 and Award No. DE-SC0021969, respectively. C. S. acknowledges a DOE Office of Science Early Career Award. This material is based upon work supported by the U.S. Department of Energy, Office of Science, Office of Nuclear Physics, within the framework of the Saturated Glue (SURGE) Topical Theory Collaboration. H. M. is supported by the Academy of Finland, the Centre of Excellence in Quark Matter, and Projects No. 338263 and No. 346567, and under the

European Union's Horizon 2020 research and innovation program by the European Research Council (ERC, Grant Agreement No. ERC-2018-ADG-835105 YoctoLHC) and by the STRONG-2020 project (Grant Agreement No. 824093). W. B. Z. is supported by the National Science Foundation (NSF) under Grant No. ACI-2004571 within the framework of the XSCAPE project of the JETSCAPE Collaboration. The content of this article does not reflect the official opinion of the European Union, and responsibility for the information and views expressed therein lies entirely with the authors. This research was done using resources provided by the Open Science Grid (OSG) [59,60], which is supported by the National Science Foundation Award No. 2030508.

[1] R. Abdul Khalek *et al.*, Science requirements and detector concepts for the Electron-Ion Collider: EIC yellow report, Nucl. Phys. **A1026**, 122447 (2022).

[2] E. C. Aschenauer, S. Fazio, J. H. Lee, H. Mäntysaari, B. S. Page, B. Schenke, T. Ullrich, R. Venugopalan, and P. Zurita, The Electron–Ion Collider: Assessing the energy dependence of key measurements, Rep. Prog. Phys. **82**, 024301 (2019).

[3] P. Agostini *et al.* (LHeC, FCC-he Study Group), The Large Hadron–Electron Collider at the HL-LHC, J. Phys. G **48**, 110501 (2021).

[4] Daniele P. Anderle *et al.*, Electron-Ion Collider in China, Front. Phys. **16**, 64701 (2021).

[5] M. G. Ryskin, Diffractive J/ψ electroproduction in LLA QCD, Z. Phys. C **57**, 89 (1993).

[6] Kari J. Eskola, Christopher A. Flett, Vadim Guzey, Topi Löytäinen, and Hannu Paukkunen, Exclusive J/ψ photoproduction in ultraperipheral Pb + Pb collisions at the CERN Large Hadron Collider calculated at next-to-leading order perturbative QCD, Phys. Rev. C **106**, 035202 (2022).

[7] Benjamin Bally *et al.*, Imaging the initial condition of heavy-ion collisions and nuclear structure across the nuclide chart, arXiv:2209.11042.

[8] Peter Filip, Richard Lednicky, Hiroshi Masui, and Nu Xu, Initial eccentricity in deformed $^{197}\mathrm{Au} + {}^{197}\mathrm{Au}$ and $^{238}\mathrm{U} + {}^{238}\mathrm{U}$ collisions at $\sqrt{s_{NN}} = 200$ GeV at the BNL Relativistic Heavy-Ion Collider, Phys. Rev. C **80**, 054903 (2009).

[9] Hiroshi Masui, Bedangadas Mohanty, and Nu Xu, Predictions of elliptic flow and nuclear modification factor from 200 GeV U + U collisions at RHIC, Phys. Lett. B **679**, 440 (2009).

[10] Tetsufumi Hirano, Pasi Huovinen, Koichi Murase, and Yasushi Nara, Integrated dynamical approach to relativistic heavy ion collisions, Prog. Part. Nucl. Phys. **70**, 108 (2013).

[11] Chun Shen, Zhi Qiu, Huichao Song, Jonah Bernhard, Steffen Bass, and Ulrich Heinz, The iEBE-VISHNU code package for relativistic heavy-ion collisions, Comput. Phys. Commun. **199**, 61 (2016).

[12] Bjoern Schenke, Prithwish Tribedy, and Raju Venugopalan, Initial-state geometry and fluctuations in Au + Au, Cu + Au, and U + U collisions at energies available at the BNL Relativistic Heavy Ion Collider, Phys. Rev. C **89**, 064908 (2014).

[13] Bjoern Schenke, Chun Shen, and Prithwish Tribedy, Running the gamut of high energy nuclear collisions, Phys. Rev. C **102**, 044905 (2020).

[14] Hao-jie Xu, Wenbin Zhao, Hanlin Li, Ying Zhou, Lie-Wen Chen, and Fuqiang Wang, Probing nuclear structure with mean transverse momentum in relativistic isobar collisions, arXiv:2111.14812.

[15] Giuliano Giacalone, Jiangyong Jia, and Chunjian Zhang, Impact of Nuclear Deformation on Relativistic Heavy-Ion Collisions: Assessing Consistency in Nuclear Physics across Energy Scales, Phys. Rev. Lett. **127**, 242301 (2021).

[16] Chunjian Zhang and Jiangyong Jia, Evidence of Quadrupole and Octupole Deformations in $^{96}\mathrm{Zr} + {}^{96}\mathrm{Zr}$ and $^{96}\mathrm{Ru} + {}^{96}\mathrm{Ru}$ Collisions at Ultrarelativistic Energies, Phys. Rev. Lett. **128**, 022301 (2022).

[17] Govert Nijs and Wilke van der Schee, Inferring nuclear structure from heavy isobar collisions using Trajectum, arXiv:2112.13771.

[18] Yi-Lin Cheng, Shuzhe Shi, Yu-Gang Ma, Horst Stöcker, and Kai Zhou, How does Bayesian analysis infer the nucleon distributions in isobar collisions?, Phys. Rev. C **107**, 064909 (2023).

[19] Wouter Ryssens, Giuliano Giacalone, Björn Schenke, and Chun Shen, Evidence of Hexadecapole Deformation in Uranium-238 at the Relativistic Heavy Ion Collider, Phys. Rev. Lett. **130**, 212302 (2023).

[20] Heikki Mäntysaari and Björn Schenke, Revealing proton shape fluctuations with incoherent diffraction at high energy, Phys. Rev. D **94**, 034042 (2016).

[21] Heikki Mäntysaari and Björn Schenke, Evidence of Strong Proton Shape Fluctuations from Incoherent Diffraction, Phys. Rev. Lett. **117**, 052301 (2016).

[22] Heikki Mäntysaari, Review of proton and nuclear shape fluctuations at high energy, Rep. Prog. Phys. **83**, 082201 (2020).

[23] Francois Gelis, Edmond Iancu, Jamal Jalilian-Marian, and Raju Venugopalan, The color glass condensate, Annu. Rev. Nucl. Part. Sci. **60**, 463 (2010).

[24] Heikki Mäntysaari, Björn Schenke, Chun Shen, and Wenbin Zhao, Bayesian inference of the fluctuating proton shape, Phys. Lett. B **833**, 137348 (2022).

[25] C. Alexa *et al.* (H1 Collaboration), Elastic and proton-dissociative photoproduction of J/ψ mesons at HERA, Eur. Phys. J. C **73**, 2466 (2013).

[26] Alfred H. Mueller, A simple derivation of the JIMWLK equation, Phys. Lett. B **523**, 243 (2001).

[27] J. P Ebran, E. Khan, T. Niksic, and D. Vretenar, How atomic nuclei cluster, Nature (London) **487**, 341 (2012).

[28] E. F. Zhou, J. M. Yao, Z. P. Li, J. Meng, and P. Ring, Anatomy of molecular structures in $^{20}\mathrm{Ne}$, Phys. Lett. B **753**, 227 (2016).

[29] P. Marević, J. P. Ebran, E. Khan, T. Nikšić, and D. Vretenar, Quadrupole and octupole collectivity and cluster structures in neon isotopes, Phys. Rev. C **97**, 024334 (2018).

[30] Mikael Frosini, Thomas Duguet, Jean-Paul Ebran, Benjamin Bally, Tobias Mongelli, Tomás R. Rodríguez, Robert Roth, and Vittorio Somà, Multi-reference many-body perturbation theory for nuclei: II. *Ab initio* study of

neon isotopes via PGCM and IM-NCSM calculations, Eur. Phys. J. A **58**, 63 (2022).

[31] B. Bally *et al.*, Deciphering small system collectivity with bowling-pin-shaped ^{20}Ne isotopes (to be published).

[32] M. L. Good and W. D. Walker, Diffraction dissociation of beam particles, Phys. Rev. **120**, 1857 (1960).

[33] Hannu I. Miettinen and Jon Pumplin, Diffraction scattering and the parton structure of hadrons, Phys. Rev. D **18**, 1696 (1978).

[34] A. Caldwell and H. Kowalski, Investigating the gluonic structure of nuclei via J/ψ scattering, Phys. Rev. C **81**, 025203 (2010).

[35] H. Kowalski, L. Motyka, and G. Watt, Exclusive diffractive processes at HERA within the dipole picture, Phys. Rev. D **74**, 074016 (2006).

[36] Yoshitaka Hatta, Bo-Wen Xiao, and Feng Yuan, Gluon tomography from deeply virtual compton scattering at small-x, Phys. Rev. D **95**, 114026 (2017).

[37] Heikki Mäntysaari and Jani Penttala, Complete calculation of exclusive heavy vector meson production at next-to-leading order in the dipole picture, J. High Energy Phys. 08 (2022) 247.

[38] Heikki Mäntysaari and Jani Penttala, Exclusive heavy vector meson production at next-to-leading order in the dipole picture, Phys. Lett. B **823**, 136723 (2021).

[39] Yuri V. Kovchegov and Eugene Levin, *Quantum Chromodynamics at High Energy*, Cambridge Monographs on Particle Physics, Nuclear Physics and Cosmology Vol. 33 (Cambridge University Press, Cambridge, England, 2022), 10.1017/9781009291446.

[40] Bjoern Schenke, Prithwish Tribedy, and Raju Venugopalan, Fluctuating Glasma Initial Conditions and Flow in Heavy Ion Collisions, Phys. Rev. Lett. **108**, 252301 (2012).

[41] Heikki Mäntysaari, Farid Salazar, and Björn Schenke, Nuclear geometry at high energy from exclusive vector meson production, Phys. Rev. D **106**, 074019 (2022).

[42] Heikki Mäntysaari, Kaushik Roy, Farid Salazar, and Björn Schenke, Gluon imaging using azimuthal correlations in diffractive scattering at the Electron-Ion Collider, Phys. Rev. D **103**, 094026 (2021).

[43] Heikki Mäntysaari and Björn Schenke, Accessing the gluonic structure of light nuclei at a future Electron-Ion Collider, Phys. Rev. C **101**, 015203 (2020).

[44] Heikki Mäntysaari, Niklas Mueller, and Björn Schenke, Diffractive dijet production and Wigner distributions from the color glass condensate, Phys. Rev. D **99**, 074004 (2019).

[45] Heikki Mäntysaari and Björn Schenke, Confronting impact parameter dependent JIMWLK evolution with HERA data, Phys. Rev. D **98**, 034013 (2018).

[46] Bjoern Schenke, Prithwish Tribedy, and Raju Venugopalan, Event-by-event gluon multiplicity, energy density, and eccentricities in ultrarelativistic heavy-ion collisions, Phys. Rev. C **86**, 034908 (2012).

[47] Jean-Paul Blaizot and Marco Claudio Traini, Effect of dipole size fluctuations on diffractive photo-production of vector mesons, arXiv:2209.15545.

[48] J. S. Moreland, J. E. Bernhard, and S. A. Bass, Alternative ansatz to wounded nucleon and binary collision scaling in high-energy nuclear collisions, Phys. Rev. C **92**, 011901(R) (2015).

[49] Mikael Frosini, Thomas Duguet, Jean-Paul Ebran, and Vittorio Somà, Multi-reference many-body perturbation theory for nuclei: I. Novel PGCM-PT formalism, Eur. Phys. J. A **58**, 62 (2022).

[50] Mikael Frosini, Thomas Duguet, Jean-Paul Ebran, Benjamin Bally, Heiko Hergert, Tomás R. Rodríguez, Robert Roth, Jiangming Yao, and Vittorio Somà, Multi-reference many-body perturbation theory for nuclei: III. *Ab initio* calculations at second order in PGCM-PT, Eur. Phys. J. A **58**, 64 (2022).

[51] Michael Bender, Paul-Henri Heenen, and Paul-Gerhard Reinhard, Self-consistent mean-field models for nuclear structure, Rev. Mod. Phys. **75**, 121 (2003).

[52] Benjamin Bally, Michael Bender, Giuliano Giacalone, and Vittorio Somà, Evidence of the Triaxial Structure of ^{129}Xe at the Large Hadron Collider, Phys. Rev. Lett. **128**, 082301 (2022).

[53] Giuliano Giacalone, Many-body correlations for nuclear physics across scales: From nuclei to quark-gluon plasmas to hadron distributions, arXiv:2305.19843.

[54] H. De Vries, C. W. De Jager, and C. De Vries, Nuclear charge and magnetization density distribution parameters from elastic electron scattering, At. Data Nucl. Data Tables **36**, 495 (1987).

[55] C. Loizides, J. Nagle, and P. Steinberg, Improved version of the PHOBOS Glauber Monte Carlo, SoftwareX **1–2**, 13 (2015).

[56] J. Carlson and R. Schiavilla, Structure and dynamics of few nucleon systems, Rev. Mod. Phys. **70**, 743 (1998).

[57] Heikki Mäntysaari and Björn Schenke, Probing subnucleon scale fluctuations in ultraperipheral heavy ion collisions, Phys. Lett. B **772**, 832 (2017).

[58] Jan Cepila, Jesus Guillermo Contreras, and Michal Krelina, Coherent and incoherent J/ψ photonuclear production in an energy-dependent hot-spot model, Phys. Rev. C **97**, 024901 (2018).

[59] Ruth Pordes *et al.*, The open science grid, J. Phys. Conf. Ser. **78**, 012057 (2007).

[60] Igor Sfiligoi, Daniel C. Bradley, Burt Holzman, Parag Mhashilkar, Sanjay Padhi, and Frank Wurthwrin, The pilot way to grid resources using glideinWMS, WRI World Congress **2**, 428 (2009).